Improvement of satellites shielding under high velocity impact using advanced SPH method

Tess LEGAUD[1], Morgan LE GARREC[1], Nicolas VAN DORSSELAER[1], Vincent LAPOUJADE[1]

[1]DynaS+ 5 avenue Didier Daurat 31400 TOULOUSE France

1 Introduction

A huge number of debris coming from human activities is currently gravitating around Earth. Their size, their nature, their orbit and their velocity can highly vary, but they all represent an increasing risk of collision and a threat for the current and future space activity [1]. The space actors are looking for solutions in order to limit these risks and to protect the structures from impacts and generation of new debris (spacecrafts conception, limitation of the debris multiplication, waste life stage strategies…).
The researches previously made as part of the European project ReVus (Reducing Vulnerability of Space Systems) highlighted that the most dangerous debris, according to the satellite mission failure probability, have a diameter included in the range 1mm to 5mm [2], [3].The collision probability with this kind of debris, although still low, is expected to significantly increase because of the increasing number of space objects.
Setting out from these results, the aim of the ATIHS project, a three years collaborative research project funded by the French region Occitanie, is to improve the satellite protection from millimetric range debris impacts. Multiple solutions exist in order to do so, ATIHS focuses on the shielding one. The project global aim consists in:

- Improving the satellites resistance on strategic locations to prevent it from the mission failure,
- Working on limiting the secondary debris generation during a non-lethal impact in order to minimize the satellite contribution to the debris increase.

The project is composed of three main tasks:

- To evaluate new innovative material solutions showing an excellent mass/resistance ratio,
- To evaluate new hypervelocity testing devices which should enable to go further than the currently available devices (goal: 8 to 12 km/s for millimetric to centimetric projectiles),
- To set up robust numerical methodologies that should make it possible to increase the capacities and the hypervelocity computations reliability, by accurately modelling the materials behaviour during this kind of extreme solicitations.

This article focuses on the numerical approach. It especially deals with the ballistic limit equations establishment, the tested materials and structures behaviour and the numerical methodologies used. As a first step, some models are built following the reference structures, such as the Whipple shield and the sandwich shield, made of two aluminium skins, separated for the second one by aluminium honeycomb, in order to evaluate the ability of the SPH method to model high velocity impacts (until 4km/s). Then, the Tillotson equation of state is set up to take into account some local sublimation phases of the materials. This user equation is then tested and validated on representative cases.

2 Numerical parameters influence for high velocity impacts

The models and the obtained results are based on the publication “Hypervelocity Impact on Spaced Target Structures: Experimental and Ouranos Simulation Achievements” from J-M Sibeaud et al. [4]. This publication shows four impact tests at 0° angle using various projectile diameters and velocities against aluminium plates. The tests performed as part of the ATIHS project focus on the third configuration, meaning that:

- The projectile diameter is 10mm,
- Its velocity is 5.941km/s,
- The impacted plate dimensions are 150mmx150mmx2mm. The plate material is aluminium 6061T6.

The publication presents some impacts on a Whipple type shield. The following parametric study only focuses on the first plate behaviour so the containment plate has not been not represented. The measures made on the model are compared to the experimental one at 16µs on:

- The debris cloud length,

- The debris velocity at the cloud front,
- The cloud maximal diameter,
- The crater diameter in the plate.

The figure below illustrates the various measures listed above and the Table 1 summarizes the experimental data extracted from the tests:

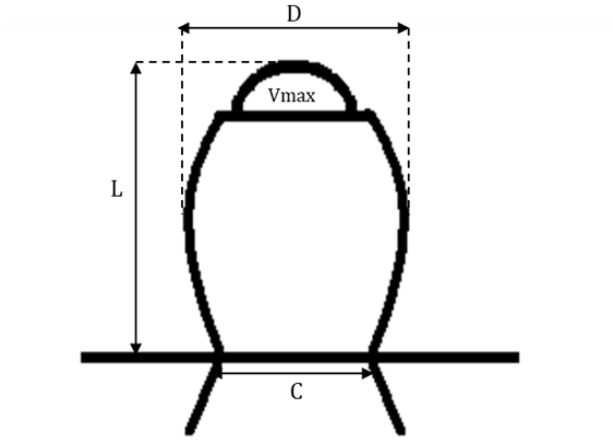

Figure 1: Illustration of the profile measurments

Mesures	Parameters	Experiment results (16µs)
Cloud maximal diameter	D	65.6 mm
Debris cloud length	L	81.1 mm
Crater diameter	C	18.9 mm
Debris velocity at the cloud front	Vmax	5.296 km/s

Table 1: Experimental measures and legends [4]

2.1 Numerical strategy of the reference model

The model represents a quarter of the experimental test, so the modelled plate dimensions are 75mmx75mmx2mm. Two symmetry planes are then used as boundary conditions. The impacted area (25mmx25mm) is modelled with SPH elements whereas the remaining area is modelled with solid lagrangian elements (reduced integration with viscous hourglass treatment). The transition SPH/Lagrange is guaranteed by a tied contact between particles and finite elements. The inter-particular length of the SPH area is 0.125mm in the three directions, which corresponds to a third of the solid elements characteristic length and to 16 SPH elements in the plate thickness. The impacting sphere is modelled with SPH and its inter-particular length is also 0.125mm. All SPH of the model use a formulation type 5 (“fluid”).

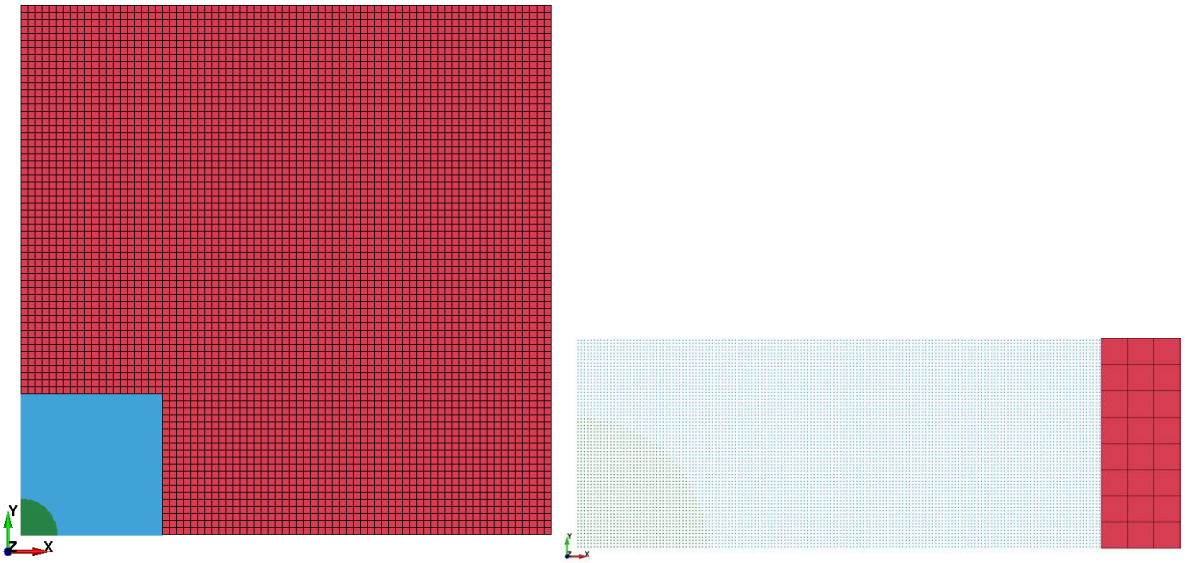

Figure 2: Illustration of the quarter model (left), zoom on the sph mesh (right)

The material behaviour law used for all parts is the Steinberg-Guinan one and the properties associated to the 6061T6 aluminium are given in the table below:

Density (g/cm3)	Shear modulus (Mbar)	Initial elastic limit (Mbar)	β factor	Exponent n	Melting elastic limit	B factor
2.703	0.276	0.0029	125	0.1	0.0068	6.52

b' factor	h factor	Atomic mass	Melting temperature (K)	a factor	Pressure cut-off (Mbar)
6.52	-6.16e-4	26.98	1220	1.5	0.02

Table 2: Parameters implemented in the Steinberg-Guinan material law

The Gruneisen equation of state is used to represent the material volumetric behaviour and the properties used in the reference model are given in the table below:

Constant parameter C	Constant parameter S1	Constant parameter S2	Constant parameter S3	Gruneisen parameter	A factor	Initial internal energy (10^e5 J)	Initial relative volume
0.524	1.4	0	0	1.97	0.48	0	0

Table 3: Parameters implemented in the Gruneisen equation of state

2.2 Results

2.2.1 Reference model

All the computations on this example are performed with the LS-DYNA R10.1 MPP double precision version. The table below summarizes the measures obtained with the reference model and its comparison with the experimental ones:

	Final crater diameter (mm)		Front debris velocity (m/s)		Cloud length (mm)		Cloud diameter (mm)	
Reference computation	18.4	2.6%	5316	-0.4%	81.3	-0.2%	69	-5.2%
Experience	18.9		5296		81.1		65.6	

Table 4: Results obtain from the reference model and comparison with the experimental test

The reference computation shows really good correlation with the experimental data, considering a maximal error of 5.2% on the cloud diameter. In order to evaluate the influence of the number of particles in the plate thickness and the influence of the SPH formulation, some additional tests are performed and are presented in the following sections.

2.2.2 Particles number in the plate thickness

According to a previous study performed by [5], the number of particles in the plate thickness is an essential numerical parameter that may generate erroneous results (or even computation crash) if it is not sufficient. This "mesh convergence study" is then crucial for the oncoming satellite shielding modelling efficiency and reliability.
The table below summarizes the results obtained with three modelling (impacted plate modelled with 12, 16 and 20 particles in its thickness). Another model using 8 particles in the plate thickness also ran but crashed before reaching the termination time.

	Final crater diameter (mm)		Front debris velocity (m/s)		Cloud length (mm)		Cloud diameter (mm)	
12 particles	20.04	-6.0%	5362	-1.2%	81.8	-0.9%	69	-5.2%
16 particles (Reference computation)	18.4	2.6%	5316	-0.4%	81.3	-0.2%	69	-5.2%
20 particles	18.7	1.1%	5398	-1.9%	81.3	-0.2%	67.4	-2.7%
Experience	18.9		5296		81.1		65.6	

Table 5: Results obtained as a function of the particle number in the plate thickness

In order to better visualize the error distribution, the graph below shows the error as a function of the considered measurement and the number of particles in the plate thickness:

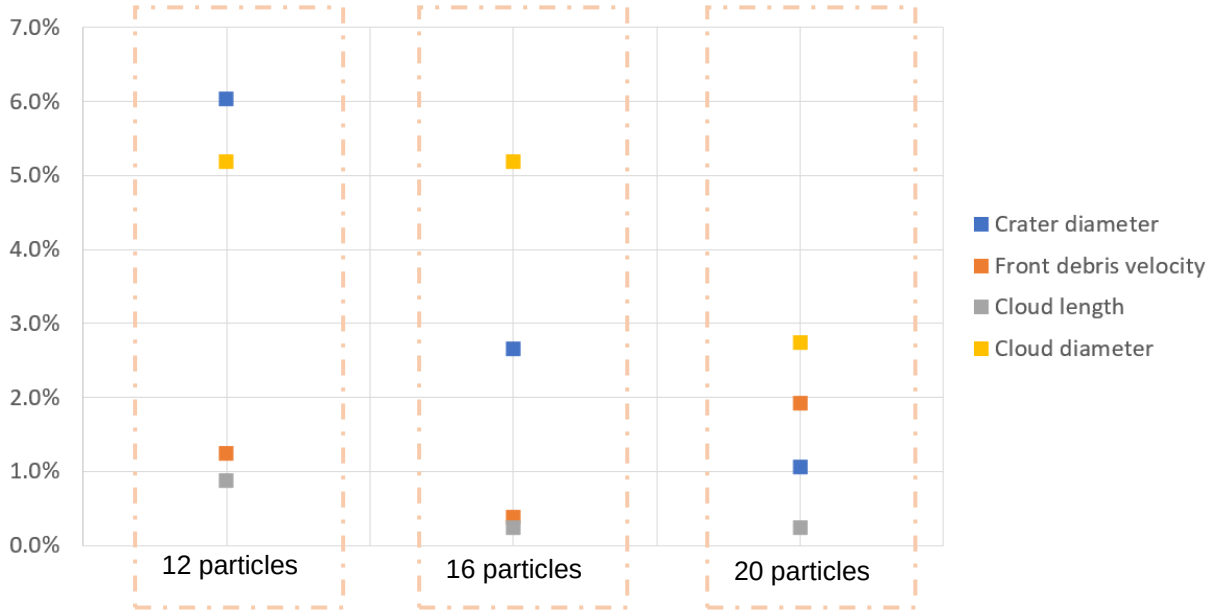

Figure 3: Diagram of the error committed on each measured parameter as a function of the particle number in the plate thickness

All the models lead to errors restricted to the range [-6%, 6%], which corresponds to accurate and reliable simulations, considering the measurement errors (user measurement, numerical artefacts, etc). However, introducing 20 particles in the plate thickness enables to reduce the range at [-3%, 3%] which characterizes an excellent correlation with the experiment. The model with 20 particles in the plate thickness enables each SPH element to use a sufficient number of neighbours to correctly predict the material behaviour. However, using 12 or 16 particles in the plate thickness remain reasonable solutions to model the plates behaviour and to minimize the calculation duration. Indeed, the model with 20 particles in the plate thickness is five times more time consuming than the 16 particles one on 8 MPP cores.

2.2.3 SPH formulation

In this study, four SPH formulations are tested in order to evaluate their influence on the plate and sphere behaviours:

- Formulation 0 which is based on the Gather approach,
- Formulation 1 which corresponds to the renormalized one using the same Gather approach as formulation 0,
- Formulation 5 which is an improved Gather approach that can better take into account high differences between materials densities,
- Formulation 6 which corresponds to the formulation 5 enhanced by the renormalization principle.

The table below summarizes the results obtained using those formulations:

	Final crater diameter (mm)		Front debris velocity (m/s)		Cloud length (mm)		Cloud diameter (mm)	
Form 0	19	-0.5%	5265	0.6%	81.1	0.0%	67.2	-2.4%
Form 1	18	4.8%	5329	-0.6%	81	0.1%	69.7	-6.3%
Form5 (Reference computation)	18.4	2.6%	5316	-0.4%	81.3	-0.2%	69	-5.2%
Form 6	18.2	3.7%	5384	-1.7%	81.2	-0.1%	68	-3.7%
Experience	18.9		5296		81.1		65.6	

Table 6: Results obtained as a function of the SPH formulation

In order to better visualize the error distribution, the graph below shows the error as a function of the considered measurement and the SPH formulation:

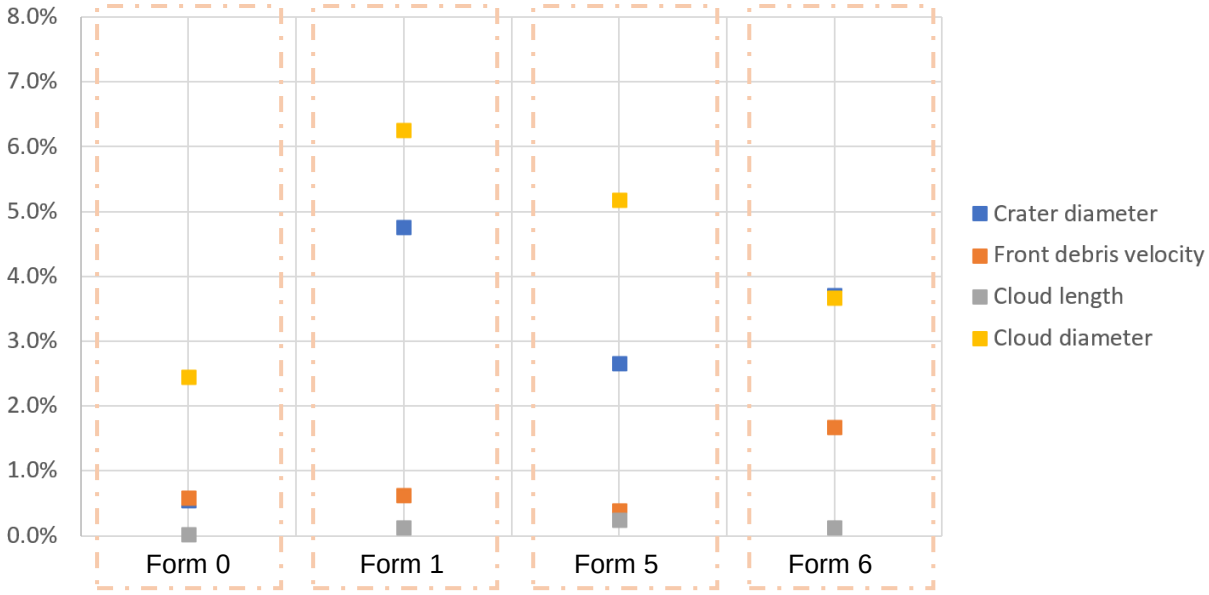

Figure 4: Diagram of the error committed on each measured parameter as a function of SPH formulation

All the models lead to errors restricted to the range [-7%, 7%], which corresponds to accurate and reliable simulations, considering the measurement errors. However, using the formulation 0 enables to reduce the range at [-3%, 3%] which characterizes an excellent correlation with the experiment.

2.2.4 Pressure cut-off

The pressure cut-off corresponds to the ultimate pressure (negative definition in those cases) from which the material is considered as failed in tensile. This parameter is a physical one and is hard to obtain. It permits the SPH method to correctly model the material behaviour and failure under high tensile strains. The table below shows the results obtained with various pressure cut off:

	Final crater diameter (mm)		Front debris velocity (m/s)		Cloud length (mm)		Cloud diameter (mm)	
100MPa	24.1	-27.5%	5284	0.2%	81.3	-0.2%	68	-3.7%
200MPa	22.4	-18.5%	5280	0.3%	81.4	-0.4%	69.6	-6.1%
1000MPa	19.7	-4.2%	5405	-2.1%	81.3	-0.2%	68.2	-4.0%
2000MPa (Reference computation)	18.4	2.6%	5316	-0.4%	81.3	-0.2%	69	-5.2%
Experience	18.9		5296		81.1		65.6	

Table 7: Results obtained as a function of the pressure cut-off

In order to better visualize the error distribution, the graph below shows the error as a function of the considered measurement and the pressure cut off:

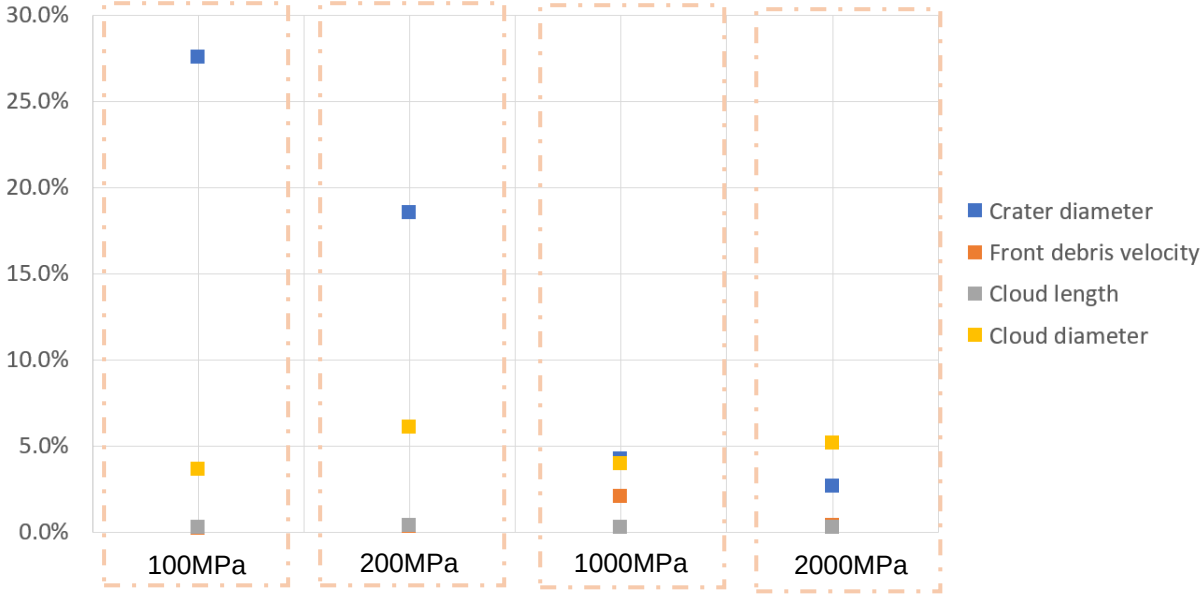

Figure 5: Diagram of the error committed on each measured parameter as a function of the pressure cut-off

The low pressures cut off (100MPa and 200MPa) do not give acceptable results considering the crater diameter measurement. However, the high pressures cut off (1000MPa and 2000MPa) enable to obtain errors lower than 6% in comparison with all the experimental measurements, which corresponds to a good correlation and reliability of the models. Those results are in accordance with the expected one, since a too low pressure cut off leads to premature failure and spalling of the material.

2.2.5 Conclusion

The quarter model enables to obtain a really great agreement with the experimental results described in [4], considering that the errors with the experimental measures remain lower than 10%. The use of 20 particles in the plate thickness, the formulation 0 and a pressure cut off equals to 1000MPa leads to an accurate and reliable model which predicts the material behaviour with a maximum error of 5%. Those modelling choices are the early stages of the ATIHS project satellite shield modelling.
The second step consists in adding the modelling of sublimation during the material response at impacts which velocities are higher than 4km/s. Next part deals with this problematic.

3 Tillotson equation of state development and validation

The Gruneisen equation of state is probably the most used equation to model materials spherical behaviour at impact velocities from some hundreds of meters per second up to six kilometres per second. The compression term enables to well predict the material spherical behaviour whereas the expansion term is not sufficient to correctly model it at extremely high strain rates. Moreover, this equation of state shows the limitation of not modelling phase changes such as sublimation that occurs during impact at velocities upper than 6km/s.
Considering the aims of the ATIHS project and the targeted impact velocities (10-12km/s), the use of the Gruneisen equation of state (EOS) has to be replaced by the use of an EOS able to model the physical behaviour occurring at extremely high strain rates. As part of the project, the Tillotson equation has been used. This equation of state is not available in LS-DYNA as an official equation, and has to be developed and used as a user equation of state.

3.1 Development

The Tillotson equation of state enables to represent the local sublimation of the material subjected to high strain rates and temperature gradients. The Tillotson equation is composed of two terms describing the material relative volume and phase changes as a function of the pressure (loading). The four regions are illustrated by the following figure [6]:

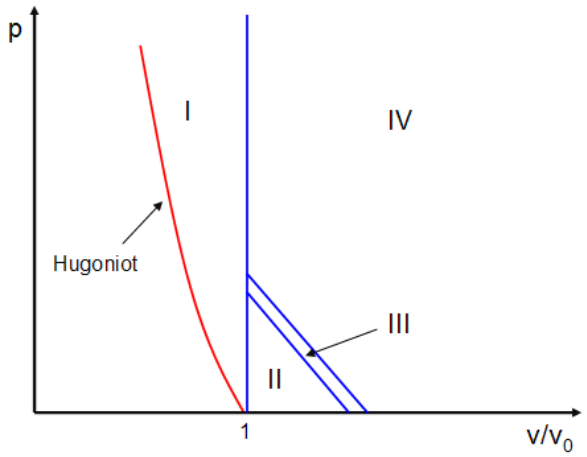

Figure 6: Phase diagram scheme [6]

Each region corresponds to a specific material phase and behaviour [7]:

- Region I corresponds to the material compressed at low pressures (from 0 to 5 Mbar). In this case, the Gruneisen equation of state is used.
- Region II corresponds to the expansion of the material having undergone a shock which energy was lower than the sublimation energy.
- Region III corresponds to a transition between Region II and Region IV (gas phase of the material). In this region, the energy produced by the shock was not sufficient to produce a change of phase in the material but the material is allowed to expand like a gas. This region ensures the continuity of the pressures and their derivatives at the boundaries between Regions II and IV. In this region the sublimation energy has to take into account an additional term proportional to the vaporization energy in order to guarantee a gas-like behaviour. In this study, the form of the equation in this region is the same as the one used to describe the material behaviour in the Region II for simplification. Moreover, the error committed is very small according to [7].
- Region IV represents the gas phase of the material.

According to [7], the pressure equation used to describe the material volumetric behaviour in regions II and III is the following:

$$aE\rho + \frac{bE\rho}{\left(\frac{E}{E_0\eta^2}+1\right)} + A\mu + B\mu^2 \qquad for\ \mu > 0\ and\ \mu < 0\ with\ E < Es$$

The pressure equation used to describe the material volumetric behaviour in region IV is:

$$aE\rho + \frac{bE\rho\exp(-\alpha(\eta^{-1}-1)^2)}{\left(\frac{E}{E_0\eta^2}+1\right)} + A\mu\exp(-\beta(\eta^{-1}-1))\exp(-\alpha(\eta^{-1}-1)^2) \qquad for\ \mu < 0\ with\ E > Es$$

Where:

Parameter	Description	Used value for aluminium 2024
ρ_0	Initial density (g/cm³)	2.785
ρ	Actual density (g/cm³)	
μ	ρ/ρ_0-1	
η	ρ/ρ_0	

A	Initial bulk modulus (Mbar)	0.75
B	Tillotson fitting parameter (Mbar)	0.65
a	Tillotson constant	0.5
b	Tillotson constant	1.63
α	Constant controlling the rate of convergence to the ideal gas	5
β	Constant controlling the rate of convergence to the ideal gas	5
E	Specific internal energy (Mbar.cm³/g)	0.05
E_s	Sublimation specific energy (Mbar.cm³/g)	0.15

Table 8: Used parameters of the Tillotson UEOS

The bulk modulus of the material has then to be updated at each loading cycle and is expressed as below:

$$G = \frac{dp}{d\rho}$$

The Tillotson equation of state has been implemented in the R11 MPP user executable.

3.2 Validation

In order to validate the implemented equation, some numerical test cases have been performed. A 3D high velocity impact model at 4km/s is presented in this paragraph to compare the results obtained with the Gruneisen and the Tillotson equations. The models are based on the reference [8], the impacting sphere diameter and the plate thickness are 0.8mm. Both sphere and plate are modelled with the same aluminium. In this validation study, only the first impacted plate is represented. The aim of this study is to compare the parameters described on the figure below between the Tillotson and the Gruneisen models.

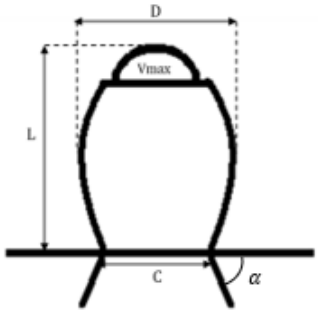

Mesures	Parameters
Cloud maximal diameter	D
Debris cloud length	L
Crater diameter	C
Debris velocity at the cloud front	Vmax
Front debris angle	α

Figure 7: Illustration of the profile measurments

In order to evaluate the material behaviour and phase at the tested impact velocities (v_0), the residual pressure (Hugoniot) generated by the shock in the target plate and in the projectile are analytically calculated, as well as the material particles velocity. The Hugoniot pressures in the projectile and in the target are equals, according to the action/reaction pinciple, and are expressed as:

$$\rho_{0t} U_{st} v_1 = \rho_{0p} U_{sp} (v_0 - v_1)$$

Where "t " refers to the target and "p" refers to the projectile. In the presented case, $\rho_{0t} = \rho_{0p} = 2.7\text{g/cm}^3$. U_s refers to the shock wave speed in the material and is expressed as:

$$U_s = c_0 + S u_p$$

Where u_p refers to the matter particle velocity and is equal to:

$$\begin{cases} v_1 & \text{in the target} \\ (v_0 - v_1) & \text{in the projectile} \end{cases}$$

The constants c_0 and S respectively are the sound speed in the unloaded material and a material dependant coefficient.

The figure below [9] shows the aluminium state (depending on the residual temperature) as a function of the particles velocity just after the shock.

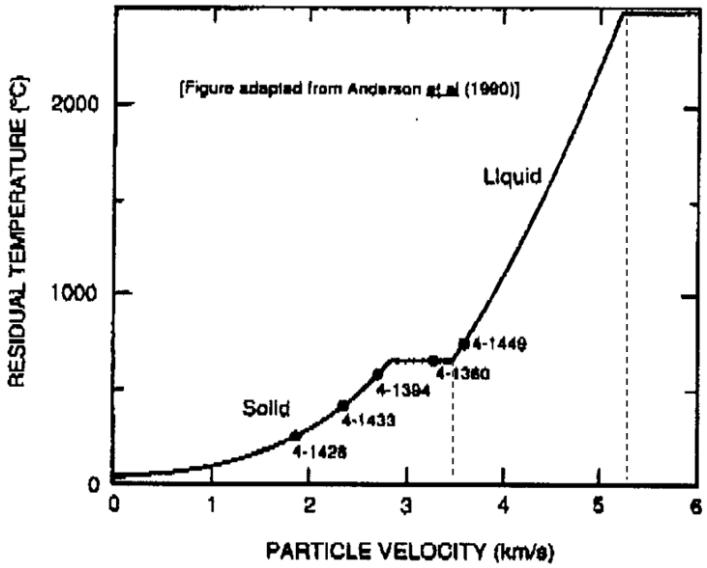

Figure 8: Evolution of the aluminium state as a function of the particle velocity and the residual temperature [9]

In order to compare the material behaviour representation of the Gruneisen and Tillotson EOS during high velocity impacts involving the solid, liquid and gas phases separatly, three computations at various impact velocities (4, 10 and 15km/s) have been run.

For each impact velocity, the Hugoniot pressure and the impacted particles velocity have been calculated and are listed in the table below:

	$v_0 = 4km/s$	$v_0 = 10km/s$	$v_0 = 15km/s$
Hugoniot pressure (Mbar)	0.43	1.65	3.80
Particles velocity (cm/µs)	0.200	0.500	0.833
Expected material state (Figure 8)	Solid	Liquid	Gas

Table 9: Description of the aluminium state and parameters as a function of the aluminium/aluminium impact velocity

The computations at 15km/s have not run yet, so they are not presented in this paper. However, those computations will be run soon and the results will be shown in the future works.

3.2.1 Impact at 4km/s

The models are compared at 10µs: the Table 10 summarizes the measured parameters for both EOS, whereas the Figure 9 ilustrates the shape of the cloud for both models. The Gruneisen model is taken as reference for this case validation becasue the reliability of this equation to model the volumetric behaviour at low pressure compressions (less than 1Mbar in this case) is excellent (see part 3.1).

	Final crater diameter (mm)	Front debris velocity (m/s)	Cloud length (mm)	Cloud diameter (mm)	Front debris angle
Gruneisen model	4.0	1690	16.1	8.7	55.9°
Tillotson model	3.9	1690	16.3	8.8	56.8°
Error	-2.5%	0%	1.2%	1.1%	1.6%

Table 10: Comparison of the aluminium behaviour modelled by a Tillotson and a Gruneisen EOS at a 4km/s impact

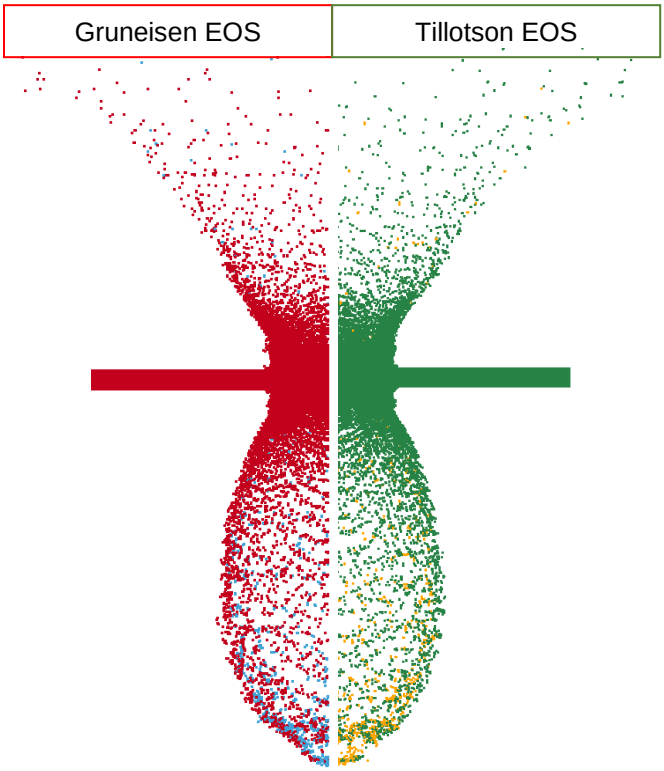

Figure 9: Comparison of the aluminium behaviour modelled by a Tillotson and a Gruneisen EOS at a 4km/s impact

The cloud shapes (front and rear) are visually almost identical and the measurement errors committed by the Tillotson model in comparison with the Gruneisen model are less than 2.5%. Thus, the Tillotson equation enables to correctly represent the volumetric behaviour at low pressure cases.
Another test is performed at 10km/s impact velocity, in order to visualize the different expansion behaviours between the Tillotson and Gruneisen models.

3.2.2 Impact at 10km/s

The models are compared at 10µs: the Table 11 summarizes the measured parameters in both cases, whereas the Figure 10 ilustrates the shape of the cloud for both models.

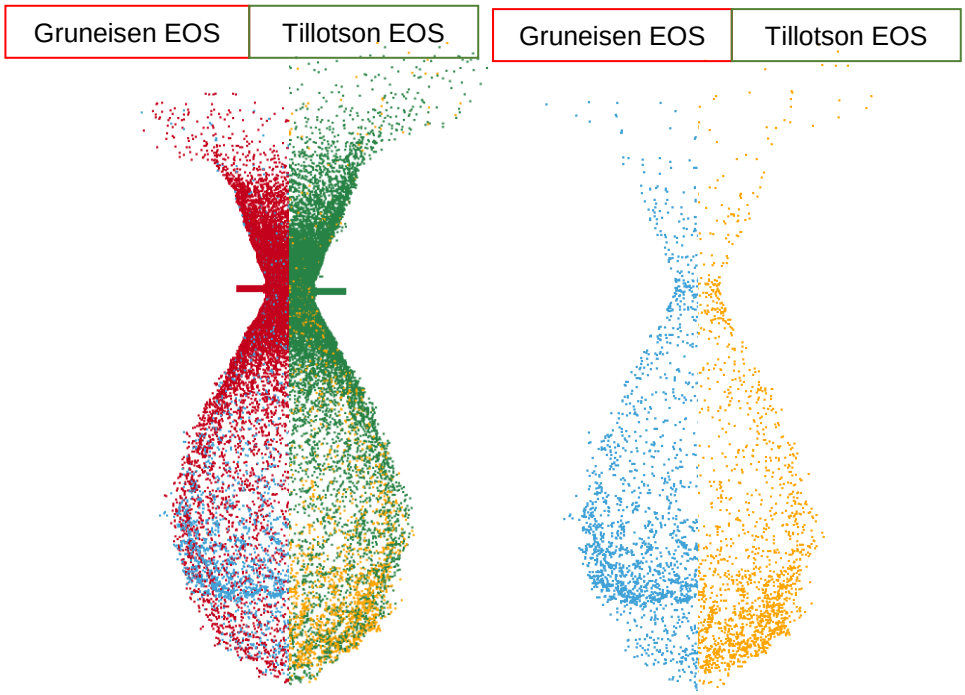

Figure 10: Comparison of the aluminium behaviour modelled by a Tillotson and a Gruneisen EOS at a 10km/s impact (all model particles on the left, sphere particles on the right)

	Final crater diameter (mm)	Front debris velocity (m/s)	Cloud length (mm)	Cloud diameter (mm)	Front debris angle
Gruneisen model	6.7	6876	69.7	41.5	71.2°
Tillotson model	6.8	6440	63.3	39.6	65.4°

Table 11: Comparison of the aluminium behaviour modelled by a Tillotson and a Gruneisen EOS at a 10km/s impact

The table above shows similar results between the Gruneisen and the Tillotson EOS whereas the Figure 10 shows a slight difference between the behaviours of the spheres in the secondary debris cloud. The Gruneisen EOS is not able to model phases changes in the matter, and the Tillotson EOS only permits to model a sudden sublimation in the matter but not the liquid phase. Those statements explain why both equations give similar results at modelling the impacted aluminium behaviour at 10km/s.

4 Ballistic Limit Equation for current satellite shields

As part of the ATIHS project, the currently used satellite shields have to be evaluated in terms of debris generation and secondary debris containment. This step has to be performed before testing new orthotropic materials developed with the aim of improving the current abilities. The studied satellite shields consist in two different configurations:

- The Whipple shield, which is composed of two aluminium skins. The space between those plates depends on the shield model.
- The sandwich shield, which is a sandwich panel composed of two aluminium skins separated by aluminium honeycomb.

The figure below illustrates the composition of those two shield types:

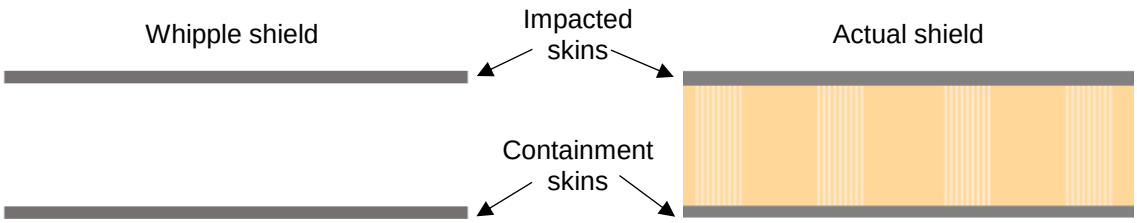

Figure 11: Description of the two studied satellite shield configurations

In both cases, the impacted skin aim is to reduce the diameter of the projectile or vaporize it, whereas the aim of the containment skin is to contain the debris without failing or spalling at its rear face. The figure below illustrates the behaviour of a containment plate subjected to the impact of the cloud generated by the impacted skin [10]. This figure shows that the impact at 8km/s generates some spalls on the containment plate rear face, and generates another debris cloud on the front face moving in the impact opposite direction.

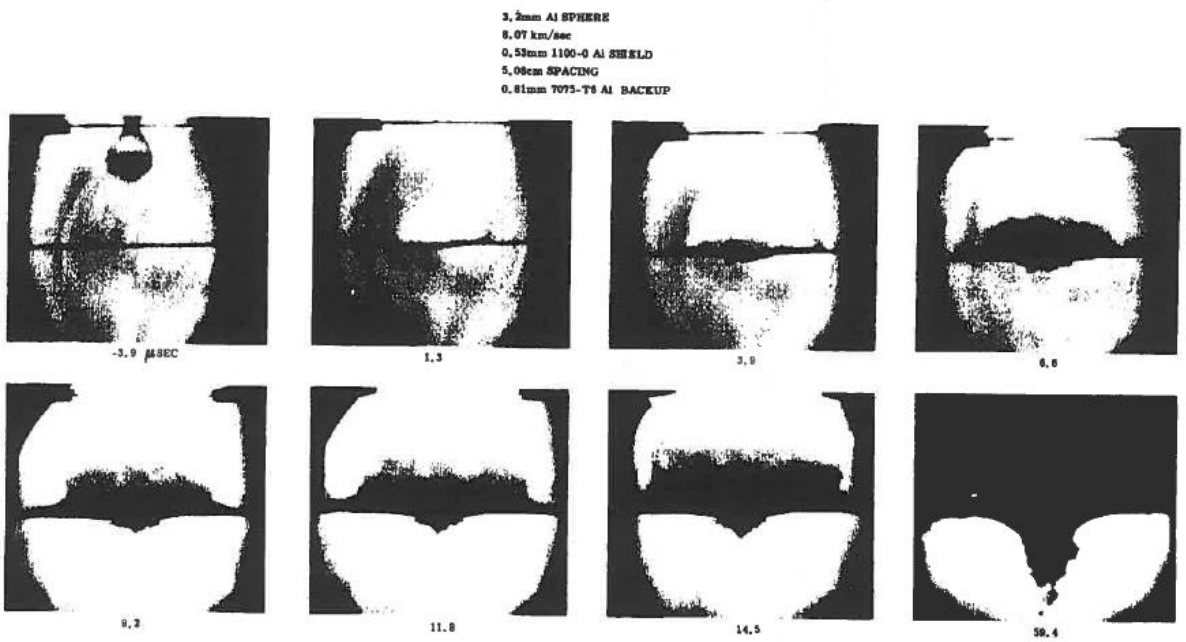

Figure 12: Evolution of the containment plate profile over time under a 8km/s impact [10]

The studied case is based on [8] and the plates are 0.8mm thick and spaced by 20mm in both shield structures. In the sandwich shield case, the honeycomb is 20mm high. The honeycomb aluminium shells are 25µm thick and the cells dimensions are 5/32. The aim of this study part is to obtain the Ballistic Limit Equation (BLE) for both shield structures, in order to evaluate the ability of the currently used shields to protect the satellite equipment from millimetric projectiles. Indeed, the BLE establishment corresponds to the projectile critical diameter as a function of its velocity. The projectile critical diameter refers to the minimal projectile diameter that induces failure or rear face spalling of the containment skin. The following figure illustrates the analytical BLE of the Whipple shield configuration described previously:

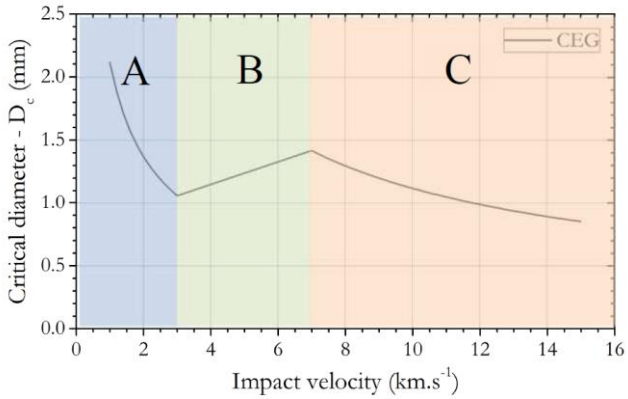

Figure 13: Analytical Ballistic Limit Equation [8]

The following sections present the results obtained for both shield configurations for the 4km/s case with two different projectile diameters (1.0mm and 1.3mm).

4.1 Projectile diameter 1.0mm

According to the Figure 13, the containment plate of the Whipple shield should not fail considering a 1.0mm diameter projectile at 4km/s. The figure below illustrates the behaviour of both shield configurations at t=16µs (Figure 14 (a), Figure 15) and at t=20µs (Figure 14 (b)).

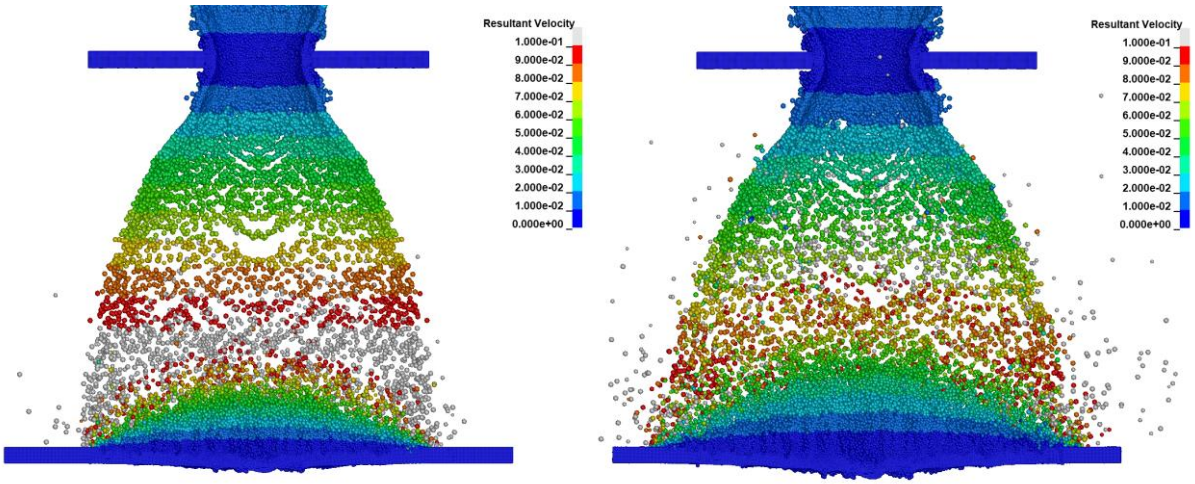

Figure 14: 1.0mm diameter impactor against the Whipple shield at t=16µs (a) and at t=20µs (b)

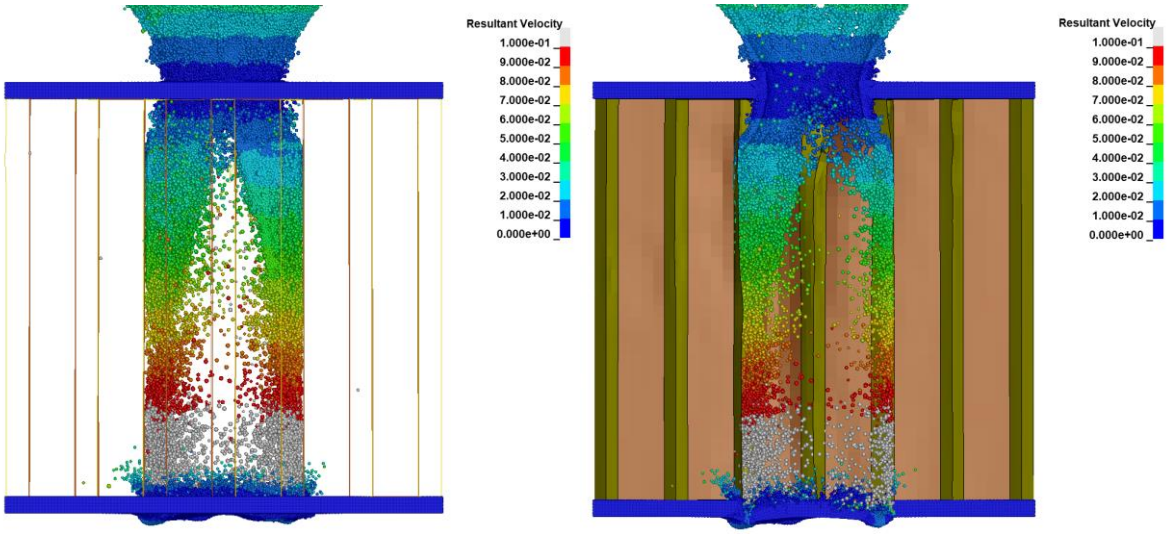

Figure 15: 1.0mm diameter impactor against the sandwich shield at t=16µs: full view (a) and at the middle cross section plane (b)

The Whipple configuration shows a high deflection of the containment plate and some craters due to heavier impacting debris, but the failure does not seem to happen according to what can be observed on the Figure 14. The Figure 16 and Figure 17 show a zoom of the most damaged area of the containment plate in both cases. On the Figure 16, the SPH particles globally remain well aligned in the plate thickness in the most energetically impacted area. This result enables to conclude to the containment plate resistance under such impact. However, the Figure 15 and Figure 17 show a clear containment plate perforation in the sandwich structure model. This means that the tunnelling effect due to the honeycomb presence leads to a more energetic and localized impact on the second plate and consequently, to a premature failure considering the analytical BLE.

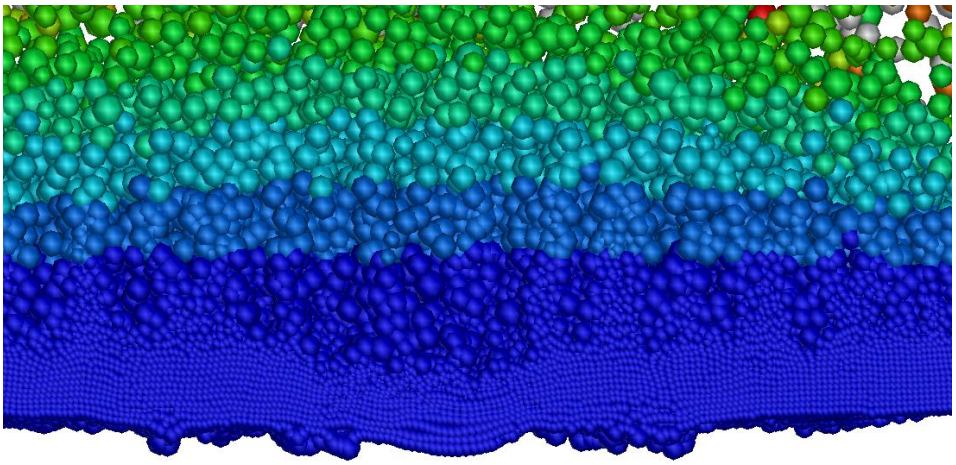

Figure 16: Zoom on the most energetically impacted area of the containement plate (Whipple shield)

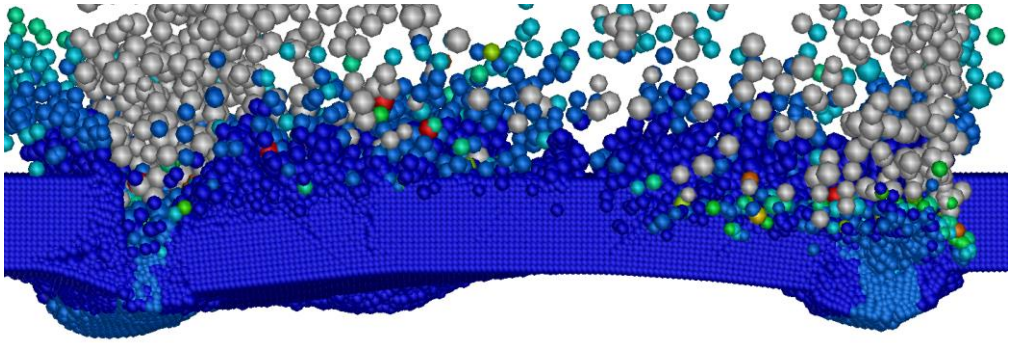

Figure 17: Zoom on the most energetically impacted area of the containement plate (sandwich shield)

4.2 Projectile diameter 1.3mm

According to the Figure 13, the containment plate should fail considering a 1.3mm diameter projectile at 4km/s. The figures below illustrate the behaviour of both shield configurations at t=13µs (Figure 18 (a), Figure 19) and at t=20µs (Figure 18 (b)).

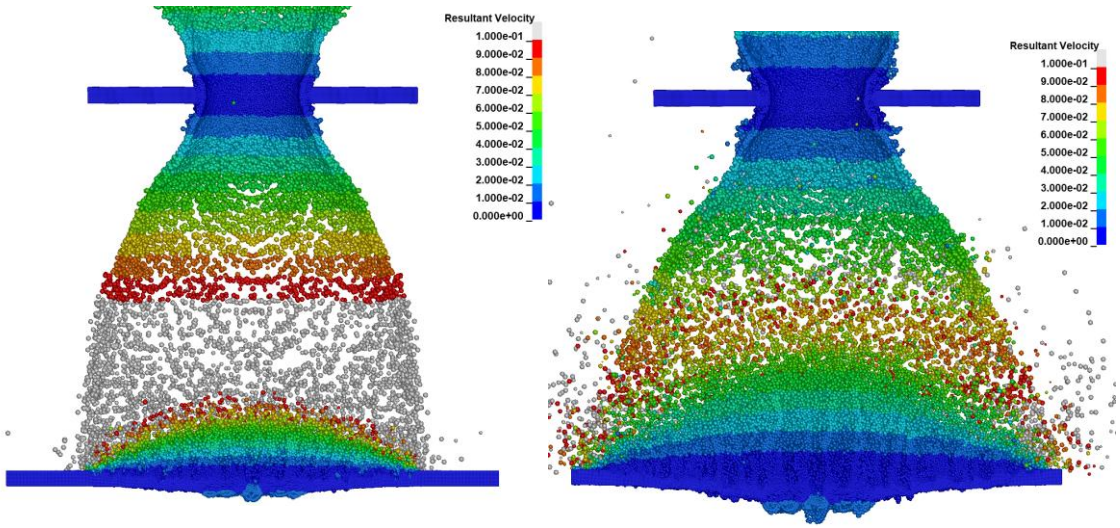

Figure 18: 1.3mm diameter impactor against the Whipple shield at t=13µs (a) and at t=20µs (b)

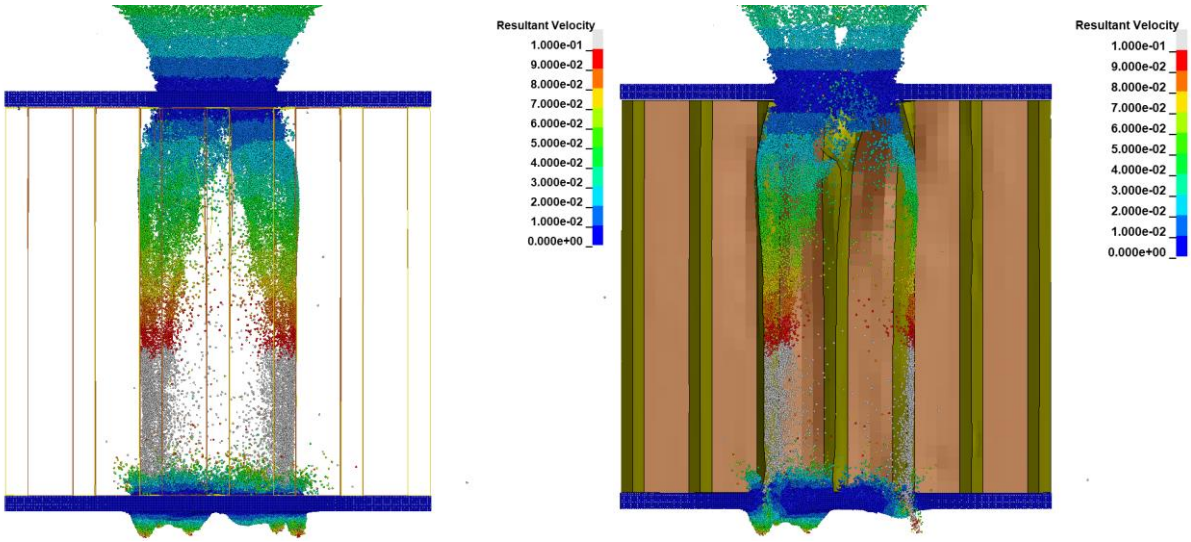

Figure 19: 1.3mm diameter impactor against the sandwich shield at t=13µs: full view (a) and at the middle cross section plane (b)

The sandwich shield shows a clear failure of the containment plate (Figure 19 and Figure 21), which is an expected result considering the failure already observed when the impactor diameter is 1mm. The Whipple configuration shows a high deflection of the containment plate and some craters due to heavier impacting debris, but the failure is not as clear as in the sandwich configuration impact case. The Figure 20 and Figure 21 show a zoom of the most damaged area of the containment plate in both cases. On the Figure 20, the SPH particles do not remain well aligned as it could be seen on the Figure 16 and a clear high disturbance occurs in all the plate thickness at the most energetically impacted area. The containment plate failure can then be concluded considering its highly damaged profile. Finally, the failure profile highly looks like the experimental profiles obtained by C.J. Maiden et al. (Figure 12) during similar high velocity impacts. Those results are then very encouraging for the future correlation to be made with the planed experimental tests.

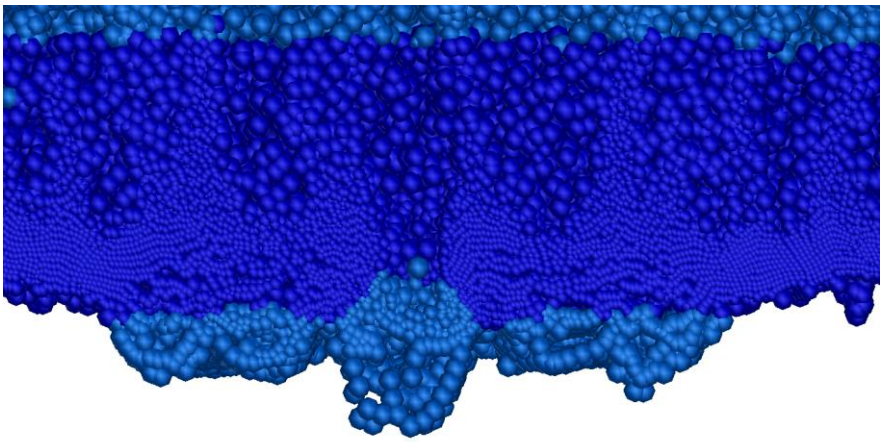

Figure 20: Zoom on the most energetically impacted area of the containement plate (Whipple shield)

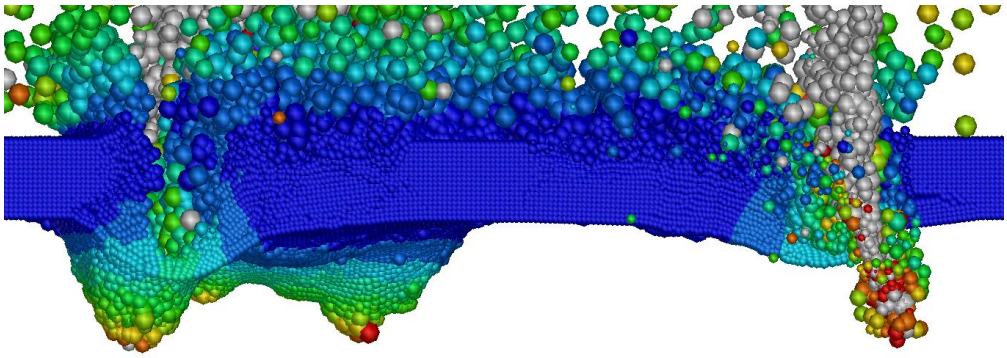

Figure 21: Zoom on the most energetically impacted area of the containement plate (sandwich shield)

4.3 Conclusion

The numerical methodology used to model both shield configurations enables to obtain accurate results on the containment plate ability to resist to the secondary debris cloud. However, those numerical tests have been performed in accordance with analytical calculations on the Whipple shield BLE. Those calculations are not perfectly reliable in those cases and some experimental tests will be performed as part of the ATIHS project. Moreover, higher velocities impacts have to be numerically modelled since the interest impact velocities of the BLE are around 10km/s. Some difficulties are currently encountered to model the impact of the secondary debris cloud on the containment plate at this range of impact velocities but will be investigated and solved soon in order to establish the numerical BLE of the Whipple and the sandwich shields. Finally, some experimental tests are needed to validate the current results and increase the reliability of those numerical results.

5 Summary

The ATIHS project numerical preamble is almost finished and the presented studies have permitted to validate some numerical approaches. As part of the project, those approaches are then reliable enough to provide experimental test tracks. The SPH number in the plates thicknesses, the pressure cut-off and the SPH formulation to use have been calibrated on experimental results [4] and the selected configuration results provide less than 5% error on four measurement types.

One of the ATIHS project aims is to establish the behaviour of the matter subjected to millimetric debris impact at velocities around 10km/s. This kind of impact cases leads to matter melting and sublimation and the Gruneisen EOS does not permit to model those phase changes. The Tillotson EOS, which enables to model sudden matter sublimation, has been implemented as a user EOS. As expected, the Tillotson and Gruneisen EOS give similar results for rather low impact velocities when the material stays in its solid and liquid phases. At higher impact velocities (~15km/s), only the implemented Tillotson EOS will be able to model the matter sublimation. However there are currently no experimental results available to validate the numerical results. An experimental campaign will be carried out soon and the EOS will be finalized in the next months.

Finally, after the establishment of the numerical parameters to model simple impact test cases, the second step consisted in modelling some millimetric debris impacts on the current Whipple and sandwich shield configurations. The aim is to establish the Ballistic Limit Equation of both shields, and compare their ability to contain the secondary debris cloud and to limit the generation of new debris at the front face. This study is currently still in process but gives encouraging results at present for impact velocities lower or equal to 4km/s. Indeed, the Whipple containment plate profile is similar to the experimental profile of C.J. Maiden et al. [10] and the points of the BLE obtained remain near the analytical ones. However, adding the honeycomb part between the plates leads to a reduction of the impactor critical diameters because of the honeycomb tunnelling effect.

The next step of the ATIHS project consists in performing experimental impact tests on the Whipple and sandwich configurations, in order to establish experimental BLE of the actual shields and to experiment the new laboratory launcher developed by Thiot Ingénierie company. Then, some innovative orthotropic materials will be tested under high velocity impacts.

6 Literature

[1] Liou J.C., Johnson N.L., Hill N.M., “Controlling the growth of future LEO debris populations with active debris removal”, Acta Astronautica, 2010; 66: 648-653

[2] Bensoussan D., “Satellite vulnerability to space debris risk”, 6th IASS Conferenc, Montreal, 2013

[3] Cougnet C., David M., Gergonne G., Oswald M., Putzar R., Stokes H., “Solutions to reduce the vulnerability of space systems to impacts of small debris particles”, 63rd international astronautical congress, Naples, Italia, september 2012.

[4] Sibeaud J.M., Héreil P.L., Albouys V., “Hypervelocity impact on spaced target structures: experimental and Ouranos simulation achievements”, International Journal of Impact Engineering 29, 2003, 647-658

[5] Beal T., Van Dorsselaer N. Lapoujade V., “A contribution to validation of SPH new features”, 9th European LS-DYNA Conference, 2013

[6]

[7] Tillotson J.H., “Metallic equations of state for hypervelocity impact”, General Atomics, 1962

[8] Deconinck P., Abdulhamid H., Héreil P.L., Mespoulet J., Puillet C., « Experimental and numerical study of submilimeter-sized hypervelocity impacts on honeycomb sandwich structures”, Procedia Enegineering, 2013

[9] Piekutowski A.J., “Characteristics of debris clouds produced by hypervelocity impact of aluminium spheres with thin aluminium plates”, University of Dayton Research Institute, 1993

[10] Maiden C.J., McMillan A.R., Sennett R.E., Gehring J.W., “Experimental investigations of simulated meteoroid damage to various spacecraft structures”, GM Defense Research Laboratories, 1965